08

Spectroscopy of the yttrium scandate doped by thulium ions

© E.A. Dobretsova, O.K. Alimov, S.Ya. Rusanov, V.V. Kashin, V.V. Voronov, D.A. Guryev, S.A. Kutovoi, V.I. Vlasov, V.B. Tsvetkov

Prokhorov Institute of General Physics, Russian Academy of Sciences, Moscow, Russia

E-mail: elenadobretsova89@gmail.com

Received July 8, 2021
Revised July 13, 2021
Accepted July 16, 2021

The thulium-doped yttrium scandate crystal fiber has been obtained by the laser-heated pedestal growth method. The crystal belongs to the bixbyite type, has a cubic structure and crystallizes in the $Ia\bar{3}$ space group. The lattice parameters ($a = 10.224(1)$ Å) have been determined using the powder X-ray diffraction. Spectral-kinetic measurements have allowed to detect two symmetrically independent optical centers of Tm^{3+} ions in the crystal fiber.

Keywords: bixbyite, optical center, rare-earth ion, laser-heated pedestal growth.

DOI: 10.21883/PSS.2022.14.54426.22s

1. Introduction

Scandium and yttrium oxides with the bixbyite structural type are characterized by high thermal conductivity (twice as high as that of yttrium aluminum garnet (YAG)) [1] and a wide spectral window from 0.25 to 9.6 μm [2]. Such properties are especially appreciated when creating solid-state lasers [3–7], so Y_2O_3 and Sc_2O_3 doped with rare-earth ions can become a worthy alternative to YAG crystals. Oxide materials are considered promising for various applications, including: solid-state light-emitting devices [8,9], high-performance luminescent materials [10,11], rare-earth magnets [12,13], materials for magnetooptical recording [14] etc.

Yttrium scandate is a polymorphic compound. Meanwhile, its high-temperature modification, as well as oxides of yttrium [15] and scandium [16], belongs to the bixbyite structural type with the space group $Ia\bar{3}$ [17]. In the crystal structure, one oxygen position with local symmetry C_1 (Wyckoff position 48*e*) and two symmetry-independent positions of cations are distinguished: with local symmetry C_{3i} (Wyckoff position 8*b*) and local symmetry C_2 (Wyckoff position 24*d*) (Fig. 1). The previous studies of the Nd^{3+}-doped $YScO_3$ crystal with the bixbyite structure type showed that Y^{3+} and Sc^{3+} are statistically distributed between two positions in a ratio of approximately 1 : 1 in each [18]. Meanwhile, Nd^{3+} freely replaces the main cations. Moreover, large octahedral voids formed between the main structural polyhedra can theoretically serve as additional positions for impurity rare-earth ions. In order to study the effect of the dopant ion radius on the structural and spectroscopic characteristics of $YScO_3$, crystal fibers of yttrium scandate doped with Tm^{3+} were synthesized and characterized in this work.

2. Experimental part

The $Tm^{3+}:YScO_3$ crystal has been synthesized by the laser-heated pedestal growth method [19,20]. This technique allows to synthesize fiber-shaped crystals and is well suited for obtaining high-melting-point materials and compounds with a disordered crystal structure, since it is accompanied by high-temperature heating and subsequent rapid cooling.

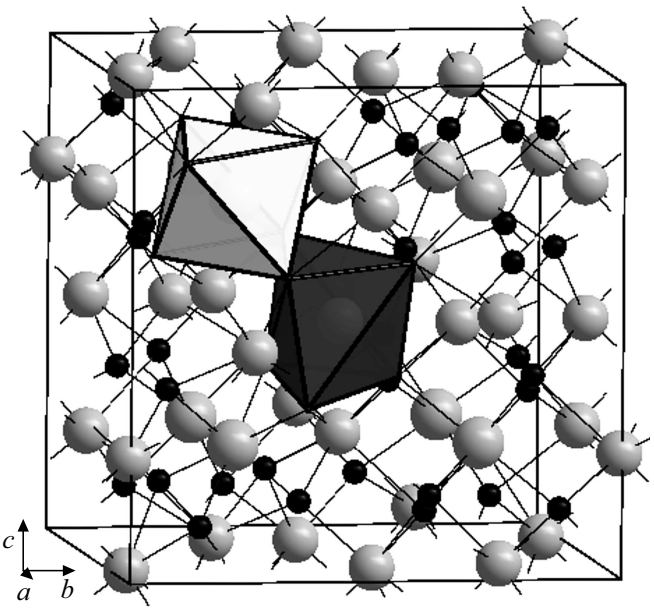

Figure 1. Crystal structure of yttrium scandate with space group $Ia\bar{3}$. Gray denotes Y^{3+} and Sc^{3+} ions statistically distributed between two symmetry-independent positions; black — oxygen ions, white and dark gray — coordination polyhedra with local symmetry C_{3i} and C_2, respectively.

Part of the resulting crystal fiber was ground in an agate mortar and characterized by the X-ray diffraction analysis. The diffraction pattern was recorded on a Bruker D8 Discover A25 DaVinsi Design X-ray diffractometer with a scanning interval of $2\theta = 15-80°$, a scanning rate of 0.02°, an exposure time of 1.0 s. A Siemens KFL ceramic X-ray tube with CuK_α radiation ($U = 40$ kV, $I = 40$ mA, $\lambda = 0.154$ nm) was used as a radiation source. The spectrum was processed using the EVA program version 2.1 and decoded using the PDF-2 database version 2011. The spectra indication and the unit cell parameters determination were carried out using the TOPAS 4.2 2 software.

The Raman spectra were recorded using an EnSpectr *R*532 portable express Raman analyzer (laser wavelength of 532 nm) equipped with an Olympus microscope. The measurements were carried out at a fortyfold magnification, focusing was carried out approximately at the core of the fiber. Each spectrum is the difference between the spectrum taken with the laser running and the dark spectrum. The subtraction of one spectrum from another was carried out automatically by the EnSpectr Pro program.

The spectral-kinetic characteristics of the $Tm^{3+}:YScO_3$ crystal fiber were obtained using laser-selective spectroscopy methods. Luminescence spectra were recorded on an MDR-23 monochromator. Hamamatsu *R*5108 photomultipliers and a Thorlabs PDA30G-EC PbS detector with amplification were used as photodetectors. A tunable laser complex LQ529B-LP 604 (Solaris LS) was used as an excitation source.

3. Results and discussion

To grow crystals, high-purity powders (> 99.999%) of scandium, yttrium, and thulium oxides (0.1 mol.%) were mixed and ground in an agate mortar to a homogeneous state. Then the mixture was placed in a platinum crucible and calcined at a temperature of 1100°C for 48 h. A rod was obtained corresponding to the composition of the powder mixture 0.1 mol.% Tm_2O_3-Y_2O_3-Sc_2O_3, about 50 mm long and 1 mm in diameter under the pressure of 20 MPa.

Top edge of the cylindrical preform (rod of composition 0.1 mol.% Tm_2O_3-Y_2O_3-Sc_2O_3), located vertically, was heated by CO_2 laser radiation. As a result, a drop of melt formed on the pedestal (the top edge of the cylindrical preform). A seed crystal was introduced into this area. Yttria-stabilized zirconia was used as a seed. At the seed contact with the melt and subsequent pulling of the crystal at a speed of 80 mm/h, a crystal fiber was formed in a shape close to cylindrical at the end of the seed. Simultaneously with the stretching of the growing crystal, the preform was fed into the heating zone to compensate for the consumption of material carried away from the melt zone by the grown fiber. As a result of the synthesis, a crystal fiber 0.6 mm in diameter and 50 mm long was obtained.

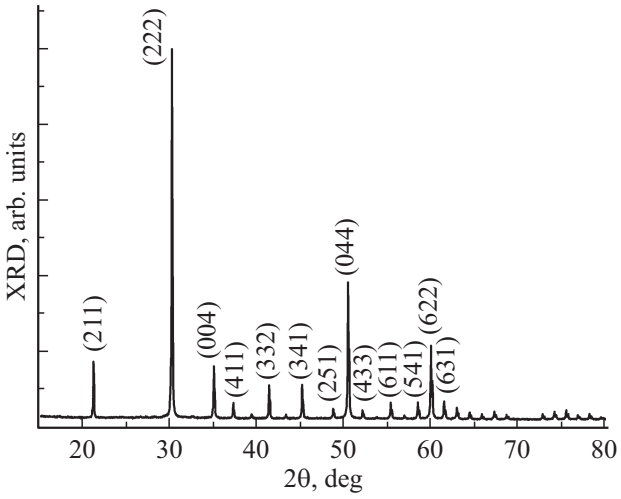

Figure 2. X-ray powder diffraction pattern of $Tm^{3+}:YScO_3$. The most intense peaks are indexed.

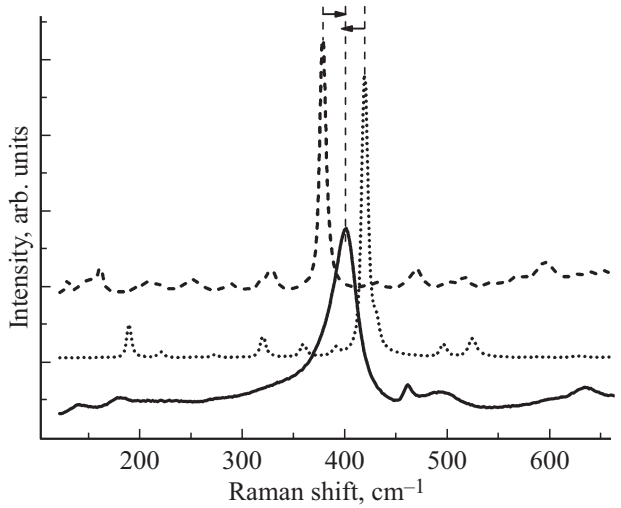

Figure 3. Raman spectra of Y_2O_3 (dashed line) and Sc_2O_3 (dotted line) and crystal fiber $Tm^{3+}:YScO_3$ (solid line).

Structural characteristics of the crystal fiber, a part of which was ground into powder, were obtained by X-ray diffraction analysis. X-ray diffraction pattern of $Tm^{3+}:YScO_3$ contains well-defined narrow peaks (Fig. 2), which indicates a high degree of crystallinity. According to X-ray diffraction data, the compound $Tm^{3+}:YScO_3$ is homogeneous and belongs to the bixbyite structural type (space group $Ia\bar{3}$), the lattice cell parameters are defined as $a = 10.224(1)$ Å. Peak indexing is shown in Table 1. The most intense peaks are indicated in Fig. 2.

The Raman spectra were obtained for the initial materials (Y_2O_3 and Sc_2O_3 powders) and crystal fibers $Tm^{3+}:YScO_3$ (Fig. 3).

The primitive cell of yttrium scandate contains 40 atoms (8 formula units). Thus, the group-theoretic analysis leads us to the following distribution of 120 phonon modes at the

Table 1. Indexing of X-ray diffraction pattern peaks $Tm^{3+}:YScO_3$. hkl — reflection indices, d — interplanar spacing, 2θ — diffraction angle, I — intensity of reflection peaks, m — multiplicity reflections.

№	h	k	l	m	d	d [18]	2θ	2θ [18]	I [18]
1	0	0	2	6		5.1083		17.346	0.36
2	2	1	1	24	4.1756	4.1709	21.261	21.285	13.54
3	0	2	2	12	3.6162	3.6121	24.598	24.626	0.04
4	2	2	2	8	2.9526	2.9493	30.246	30.28	100.00
5	3	2	1	24	2.7336	2.7305	32.734	32.772	0.07
6	2	3	1	24	2.7336	2.7305	32.734	32.772	0.03
7	0	0	4	6	2.5570	2.5542	35.065	35.106	18.45
8	4	1	1	24	2.4108	2.4081	37.268	37.312	4.62
9	0	4	2	12	2.2871	2.2845	39.365	39.411	0.48
10	4	0	2	12	2.2871	2.2845	39.365	39.411	0.73
11	3	3	2	24	2.1806	2.1782	41.372	41.421	8.36
12	4	2	2	24	2.0878	2.0855	43.302	43.353	1.03
13	3	4	1	24	2.0059	2.0036	45.166	45.219	5.15
14	4	3	1	24	2.0059	2.0036	45.166	45.219	3.96
15	2	5	1	24	1.8674	1.8653	48.724	48.782	1.79
16	5	2	1	24	1.8674	1.8653	48.724	48.782	1.48
17	0	4	4	12	1.8081	1.8061	50.432	50.492	47.56
18	4	3	3	24	1.7541	1.7521	52.098	52.161	2.14
19	0	0	6	6	1.7047	1.7028	53.728	53.793	0.40
20	4	4	2	24	1.7047	1.7028	53.728	53.793	0.07
21	6	1	1	24	1.6592	1.6574	55.324	55.392	3.47
22	3	5	2	24	1.6592	1.6574	55.324	55.392	0.96
23	5	3	2	24	1.6592	1.6574	55.324	55.392	1.15
24	0	6	2	12	1.6172	1.6154	56.890	56.96	0.78
25	6	0	2	12	1.6172	1.6154	56.890	56.96	0.42
26	5	4	1	24	1.5782	1.5765	58.429	58.501	2.68
27	4	5	1	24	1.5782	1.5765	58.429	58.501	1.86
28	6	2	2	24	1.5419	1.5402	59.942	60.017	27.23
29	6	3	1	24	1.5081	1.5064	61.433	61.51	3.43
30	3	6	1	24	1.5081	1.5064	61.433	61.51	3.13
31	4	4	4	8	1.4763	1.4746	62.903	62.982	3.66
32	4	5	3	24	1.4465	1.4448	64.354	64.435	0.60
33	5	4	3	24	1.4465	1.4448	64.354	64.435	1.27
34	0	6	4	12	1.4184	1.4168	65.788	65.871	1.13
35	6	0	4	12	1.4184	1.4168	65.788	65.871	0.22
36	7	2	1	24	1.3919	1.3903	67.205	67.291	1.09
37	2	7	1	24	1.3919	1.3903	67.205	67.291	1.99
38	6	3	3	24	1.3919	1.3903	67.205	67.291	0.77
39	5	5	2	24	1.3919	1.3903	67.205	67.291	0.01
40	6	4	2	24	1.3668	1.3653	68.608	68.696	0.23
41	4	6	2	24	1.3668	1.3653	68.608	68.696	1.28
42	7	3	2	24	1.2990	1.2975	72.741	72.836	0.08
43	5	6	1	24	1.2990	1.2975	72.741	72.836	0.00
44	3	7	2	24	1.2990	1.2975	72.741	72.836	0.97
45	6	5	1	24	1.2990	1.2975	72.741	72.836	0.80
46	0	0	8	6	1.2785	1.2771	74.098	74.195	4.70
47	8	1	1	24	1.2590	1.2576	75.445	75.545	1.74
48	4	7	1	24	1.2590	1.2576	75.445	75.545	0.76
49	7	4	1	24	1.2590	1.2576	75.445	75.545	0.58
50	5	5	4	24	1.2590	1.2576	75.445	75.545	0.54
51	0	8	2	12	1.2403	1.2389	76.784	76.886	0.54
52	8	0	2	12	1.2403	1.2389	76.784	76.886	0.92
53	6	4	4	24	1.2403	1.2389	76.784	76.886	0.46
54	6	5	3	24	1.2225	1.2211	78.116	78.221	1.04
55	5	6	3	24	1.2225	1.2211	78.116	78.221	1.07
56	0	6	6	12	1.2054	1.204	79.441	79.548	1.34
57	8	2	2	24	1.2054	1.204	79.441	79.548	0.03

$\Gamma = 0$ point of the Brillouin zone [21,22]:

$$\Gamma = (3A_g + 3A_u + 3E_g + 3e_u + 9F_g + 9F_u) \text{ (local symmetry } C_1)$$
$$+ (A_g + A_u + E_g + E_u + 5F_g + 5F_u) \text{ (local symmetry } C_2)$$
$$+ (A_u + E_u + 3F_u) \text{ (local symmetry } C_{3i}(S_6)).$$

After subtracting $1F_u$ acoustic modes, there are $16F_u$ IR-active, $(A_g + 4E_g + 14F_g)$ Raman-active and $(5A_u + 5E_u)$ optically inactive phonon modes.

In the series $Sc_2O_3 \rightarrow YScO_3 \rightarrow Y_2O_3$ there is the „mass effect“, in which the vibrational modes are shifted to a lower frequency area with an increase in the cation mass. The spectral lines of yttrium scandate are broadened, probably due to the presence of both Y^{3+} and Sc^{3+} ions statistically distributed between two positions in the bixbyite crystal structure. Due to partial overlap, the number of lines in the experimental spectrum of the scandate crystal is much lower than the number of lines predicted by the group-theoretical analysis. Table 2 shows the identification of Raman-active vibrations [23].

Luminescence excitation spectra of Tm^{3+} at the $^3H_6 \rightarrow {}^3H_5$ transition with selective recording of spectra at 1945 nm (transition $^3F_4 \rightarrow {}^3H_6$) were obtained at a temperature of 77 K (Fig. 4). The spectra show two most intense peaks at 1202.4 and 1209.4 nm. The ratio of the intensities of these spectral lines varies depending on the time delay of detection relative to the moment of laser excitation, which allows to denote the presence of two types of thulium optical centers with different lifetimes in the $YScO_3$ crystal. It is known [24] that electric dipole transitions are forbidden for rare-earth ions located in centrosymmetric positions, in particular, in the C_{3i} position in the bixbyite structure, and luminescence from such centers should not be observed. The presence of the second optical center is due to local disorder [25] in

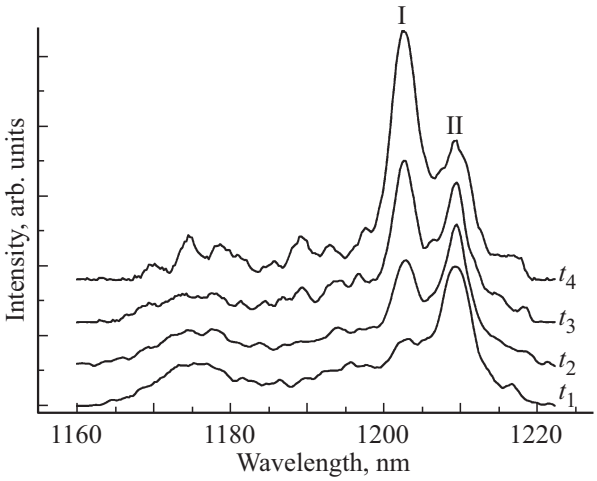

Figure 4. Luminescence excitation spectrum $Tm^{3+}:YScO_3$ (time delays $t_1 = 0.6$ ms, $t_2 = 6$ ms, $t_3 = 10$ ms, $t_4 = 12$ ms).

Table 2. RRS-active vibrations in Y_2O_3, Sc_2O_3 and $Tm^{3+}:YScO_3$; exp. — experimental, calc. — calculated

Assignments [23]	Sc_2O_3, exp. [23]	Sc_2O_3, calc. [23]	Sc_2O_3	$YScO_3$	Y_2O_3, exp. [23]	Y_2O_3, calc. [23]	Y_2O_3
Ag	221	220	220	180	162	162	161
	391	351	358	–	–	306	318
	495	498	494	–	431	460	467
	623	593	–	590	–	553	542
E_g	273	273	273	–	194	198	194
	359	332	–	–	325	290	288
	430	416	429	400	–	366	358
	626	590	–	–	–	555	567
F_g	189	192	189	140	129	132	129
	202	199	–	180	138	138	152
	252	250	253	–	182	181	207
	319	306	–	–	235	234	217
	329	311	319	–	–	244	250
	359	341	358	–	325	288	288
	–	368	–	–	–	299	–
	391	386	390	–	–	338	327
	419	412	418	400	377	368	377
	–	472	–	460	–	416	429
	–	491	494	–	–	442	467
	523	536	522	495	469	495	499
	587	605	624	590	–	545	514
	669	646	670	630	592	581	592

the position with C_{3i} symmetry when the Tm^{3+} ion enters this matrix, as a result of which the symmetry decreases and the position becomes non-centrosymmetric. A similar pattern was observed in a crystal of yttrium scandate doped with Nd^{3+} [18]. Therefore, we can conclude that the nature of the distribution of a rare-earth impurity into the crystal structure of a given compound does not depend on the radius of the impurity ion.

4. Conclusion

$Tm^{3+}:YScO_3$ crystal fiber with the bixbyite structure type was obtained by the laser-heated pedestal growth method. X-ray diffraction data indicate the homogeneity of the sample and a high degree of crystallinity. The results of the analysis of the Raman spectra indicate the statistical distribution of the main cations Y^{3+}, Sc^{3+} between two cationic positions with symmetry C_{3i} (centrosymmetric) and C_2 (non-centrosymmetric) in the bixbyite structure. Selective laser spectroscopy methods revealed two types of optical centers of Tm^{3+} ions located in non-centrosymmetric positions. The nature of the appearance of the second optical center is associated with partial local disordering in positions with C_{3i} symmetry when the Tm^{3+} impurity ion enters the crystal structure. A comparison of two $YScO_3$ crystals doped with Nd^{3+} and Tm^{3+} showed that the spectral behavior of rare-earth impurities in a crystal does not depend on their ionic radius.

Acknowledgments

X-ray diffraction measurements were carried out using the equipment of the Research Equipment Sharing Center of the GPI RAS.

Work funding

The work was carried out with the support of a grant Russian Science Foundation, grant number 22-22-00968.

Conflict of interest

The authors declare that they have no conflict of interest.

References

[1] P.H. Klein, W.J. Croft. J. Appl. Phys. **38**, *4*, 1603 (1967).
[2] Y. Nigara. Jpn J. Appl. Phys. **7**, *4*, 404 (1968).
[3] K. Petermann. In: Handbook of Solid-State Lasers. Elsevier (2013). P. 3-27.
[4] L. Fornasiero, E. Mix, V. Peters, K. Petermann, G. Huber. Cryst. Res. Technol.: J. Exp. Industrial Cryst. **34**, *2*, 255 (1999).
[5] Z. Zhou, X. Guan, X. Huang, B. Xu, H. Xu, Z. Cai, X. Xu, P. Liu, D. Li, J. Zhang, J. Xu. Opt. Lett. **42**, *19*, 3781 (2017).
[6] W. Liu, D. Lu, R. Guo, K. Wu, S. Pan, Y. Hang, D. Sun, H. Yu, H. Zhang. J. Wang. Cryst. Growth Des. **20**, *7*, 4678 (2020).
[7] S. Li, L. Zhang, X. Tan, W. Deng, M. He, G. Chen, M. Xu, Y. Yang, S. Zhang, P. Zhang, Z. Chen, Y. Hang. Opt.Mater. **96**, 109277 (2019).

[8] M.M. Antoinette, S. Israel, A.J. Amali, J.L. Berchmans, B.S. Kumar, G. Manoj, U.M. Usmaniya. Nano-Struct. Nano-Objects **13**, 51 (2018).
[9] K.R. Devi, S.D. Singh, T.D. Singh. Indian J. Phys. **92**, *6*, 725 (2018).
[10] E.W. Barrera, C. Cascales, M.C. Pujol, K.H. Park, S.B. Choi, F. Rotermund, J.J. Carvajal, X. Mateos, M. Aguiló, F. Díaz. Phys. Proc. **8**, 142 (2010).
[11] A. Kumar, S. Tiwari, K. Kumar, V. Rai. Spectrochim. A **167**, 134 (2016).
[12] K.P. Tseng, Q. Yang, S.J. McCormack, W.M. Kriven. J. Am. Ceram. Soc. **103**, *1*, 569 (2020).
[13] K.E. El-Kelany, C. Ravoux, J. Desmarais, P. Cortona, Y. Pan, J. Tse, A. Erba. Phys. Rev. B **97**, *24*, 245118 (2018).
[14] S. Balabanov, S. Filofeev, M. Ivanov, E. Kalinina, D. Kuznetsov, D. Permin, E. Rostokina. Heliyon **5**, *4*, e01519 (2019).
[15] F. Hanic, M. Hartmanová, G. Knab, A. Urusovskaya, K.S. Bagdasarov. Acta Crystallographica B **40**, *2*, 76 (1984).
[16] S. Geller, P. Romo, J. Remeika. Z. Kristallograph. Cryst. Mater. **124**, *1–6*, 136 (1967).
[17] J. Clark, P. Richter, L. Du Toit. J. Solid State Chem. **23**, *1–2*, 129 (1978).
[18] O. Alimov, E. Dobretsova, D. Guryev, V. Kashin, G. Kiriukhina, S. Kutovoi, S. Rusanov, S. Simonov, V. Tsvetkov, V. Vlasov, V. Voronov, O. Yakubovich. Cryst. Growth Des. **20**, *7*, 4593 (2020).
[19] G.A. Bufetova, V.V. Kashin, D.A. Nikolaev, S.Y. Rusanov, V.F. Seregin, V.B. Tsvetkov, I.A. Shcherbakov, A.A. Yakovlev. Quantum Electron. **36**, *7*, 616 (2006).
[20] R.S. Feigelson. J. Cryst. Growth **79**, *1–3*, 669 (1986).
[21] W.B. White, V.G. Keramidas. Spectrochim. Acta A **28**, *3*, 501 (1972).
[22] D.L. Rousseau, R.P. Bauman, S. Porto. J. Raman Spectroscopy **10**, *1*, 253 (1981).
[23] M.V. Abrashev, N.D. Todorov, J. Geshev. J. Appl. Phys. **116**, *10*, 103508 (2014).
[24] A.A. Kaminsky. Lazernye kristally. Nauka, M. (1975) (in Russian).
[25] O.K. Alimov, T.T. Basiev, S.B. Mirov. Tr. GPI RAS, **9**, 6 (1987) (in Russian).